analytical chemistry

pubs.acs.org/ac

Article

# SCORe: SARS-CoV-2 Omicron Variant RBD-Binding DNA Aptamer for Multiplexed Rapid Detection and Pseudovirus Neutralization

Lucy F. Yang, Nataly Kacherovsky, Joey Liang, Stephen J. Salipante, and Suzie H. Pun*

Cite This: https://doi.org/10.1021/acs.analchem.2c01993

Read Online

ACCESS | Metrics & More | Article Recommendations | Supporting Information

**ABSTRACT:** During the COVID-19 (coronavirus disease 2019) pandemic, several SARS-CoV-2 variants of concern emerged, including the Omicron variant, which has enhanced infectivity and immune invasion. Many antibodies and aptamers that bind the spike (S) of previous strains of SARS-CoV-2 either do not bind or bind with low affinity to Omicron S. In this study, we report a high-affinity **S**ARS-**C**oV-2 **O**micron **R**BD-binding aptam**e**r (SCORe) that binds Omicron BA.1 and BA.2 RBD with nanomolar $K_{D1}$. We employ aptamers SCORe.50 and SNAP4.74 in a multiplexed lateral flow assay (LFA) to distinguish between Omicron and wild-type S at concentrations as low as 100 pM. Finally, we show that SCORe.50 and its dimerized form SCOReD can neutralize Omicron S-pseudotyped virus infection of ACE2-overexpressing cells by >70%. SCORe therefore has potential applications in COVID-19 rapid diagnostics as well as in viral neutralization.

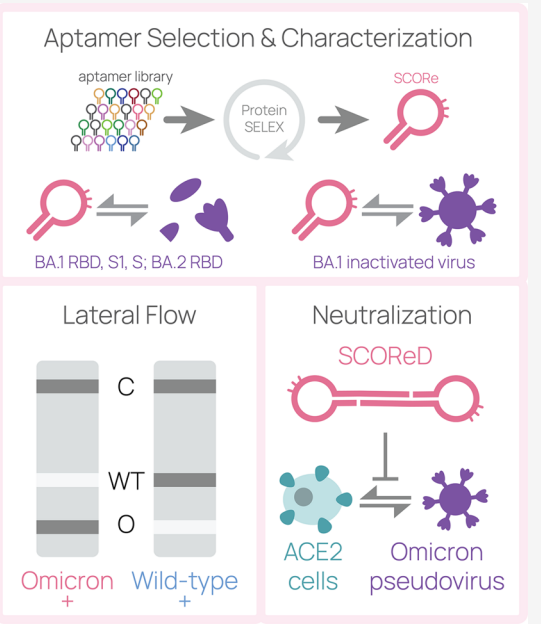


First identified to infect humans in 1967, the coronavirus subfamily has low pathogenic strains, such as HCoV-OC43, and severe disease-causing strains, such as SARS-CoV and SARS-CoV-2.[1] The evolution rate of coronavirus is impacted by its large RNA-based genome, low fidelity of viral polymerase, and recombination with other coronavirus variants within the host.[1] SARS-CoV-2, the pathogen responsible for the ongoing COVID-19 pandemic, has already evolved since its initial characterization in 2019. The World Health Organization has five SARS-CoV-2 variants as "variants of concern" (VOC) due to their increased global health significance: Alpha (B.1.1.7), Beta (B.1.351), Gamma (P.1), Delta (B.1.617.2), and Omicron (B.1.1529 AKA BA.1, BA.2) strains.[2] First detected in November 2021, Omicron variant SARS-CoV-2 has both improved immune evasion and more efficient spread compared to the ancestral virus.[3,4] Plasma from both convalescent and vaccinated individuals has less neutralizing activity against Omicron pseudovirus versus earlier strains. In addition, the Omicron strain binds with a 2.4-fold higher affinity to the angiotensin-converting enzyme-2 (ACE2) receptor compared with wild-type Wuhan-Hu-1 virus.[3]

The SARS-CoV-2-enveloped virus has a lipid shell containing a spike protein (S protein or S), a trimeric glycosylated protein that mediates virus binding to angiotensin-converting enzyme-2 (ACE2) on host cells. Each S monomer is comprised of the exposed subunit 1 (S1) connected to the membrane-anchored subunit 2 (S2) by a furin cleavage sequence.[5] S1 contains both the critical receptor-binding domain (RBD) that contacts the ACE2 receptor through the receptor-binding motif (RBM, residues 438−506) as well as the amino-terminal domain (NTD). S1 is the primary target for SARS-CoV-2-neutralizing antibodies, which have been reported to bind both the RBD and NTD domains of SARS-CoV-2 S protein.[6]

Molecular recognition agents that bind new variants are critical for the rapid detection of SARS-CoV-2 in patient samples as well as in emerging technologies to sense intact virus in the environment. The two major types of molecular

**Received:** May 6, 2022
**Accepted:** August 3, 2022

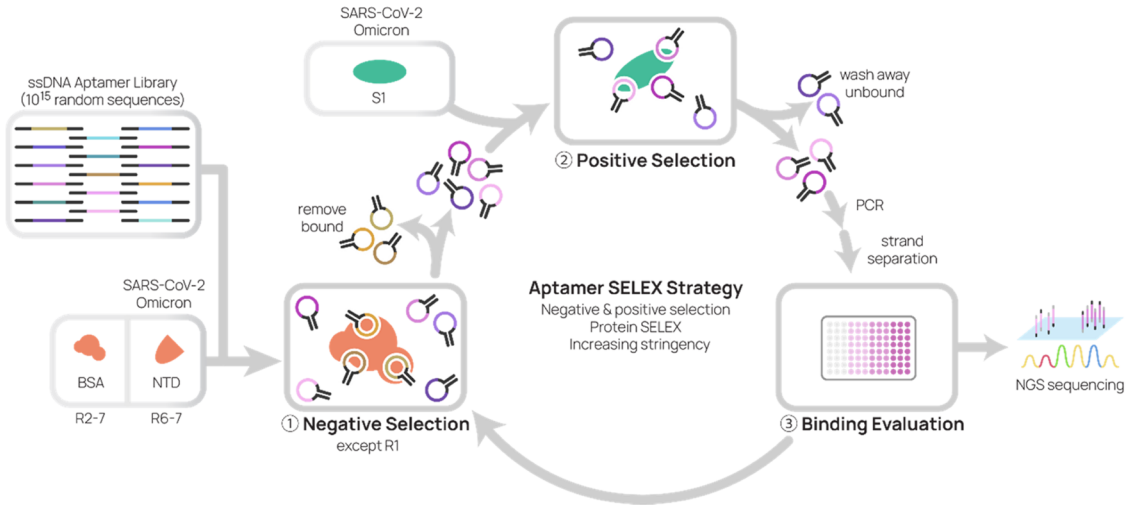


**Figure 1.** Schematic of the SELEX process. A single-stranded DNA (ssDNA) aptamer library is subjected to SARS-CoV-2 Omicron (BA.1) S1 protein for seven rounds of positive selection with increasing stringency and SARS-CoV-2 Omicron (BA.1) NTD negative selection in rounds 6 and 7 only. Binding of aptamer round pool is evaluated by protein-binding assay, and aptamer round pools with positive binding are sequenced and analyzed.

recognition agents are antibodies and aptamers, which are nucleic acid sequences that fold into secondary structures. Aptamers have target binding affinities on par with antibodies while offering several advantages such as small size and extended shelf life.[7] As chemically synthesized agents, aptamers are also produced more affordably and reproducibly than antibodies[8] and are therefore well suited for rapid viral detection assays. Numerous platforms for aptamer-based SARS-CoV-2 detection have been reported, including electrochemical sensors,[9,10] ion transport-sensing nanopores,[11] metal nanostructure-based optical sensing,[12] and lateral flow assays (LFAs), which provide rapid, point-of-care results from patient samples.[13,14]

DNA aptamers against SARS-CoV-2 S protein have been identified using a library selection process called the systematic evolution of ligands by exponential enrichment (SELEX).[15] Most of the currently reported aptamers were selected against wild-type or alpha variant S protein.[13,16−19] To the best of our knowledge, only the Li group has reported a DNA aptamer that binds to BA.1 S protein[20] that does not also bind nonspecifically to His-tag-containing proteins (Figure S1A). We tested literature-reported S-binding aptamers (SP6.51,[18] SNAP1,[13] SNAP4.74,[14] CoV-2-4C,[19] CoV-2-6C3[21]), including two discovered by our group, but none of these aptamers show specific binding to BA.1 NTD or S1 protein (Figure S1) in our testing conditions.[13,14,18] While the CoV-2-4C[19] and CoV-2-6C3[21] aptamers showed binding to BA.1 NTD, S1, and RBD proteins, they also showed binding to a control, His-tagged protein (Figure S1A), an observation also noted by Schmitz et. al.[18]

In this work, we report a **S**ARS-**C**oV-2 **O**micron variant **R**BD-binding aptame**r** (SCORe) identified in protein SELEX using BA.1 S1 protein. Biolayer interferometry (BLI) measurements reveal that SCORe and its truncation SCORe.50 bind BA.1 RBD with a $K_{D1}$ of 1.73 and 2.80 nM, respectively, and that SCORe.50 binds BA.2 RBD with 2.86 nM affinity. We demonstrate a proof-of-concept rapid lateral flow assay (LFA) that uses SCORe.50 and SNAP4.74 to differentiate between BA.1 and wild-type SARS-CoV-2 S protein. Lastly, we show that monomeric SCORe.50 as well as SCORe.50 dimers (SCOReD) can reduce the BA.1 S-pseudotyped virus infection of ACE2-expressing human cells by over 70%.

## EXPERIMENTAL SECTION

**Oligonucleotides.** All oligonucleotides were synthesized by Integrated DNA Technologies. The ssDNA library used in the protein SELEX process was 5′-TCGCTCTTTC CGCTT-CTTCGCGG-N40-CCGCGTAAGTCCGTGTGTGCGAA-3′. The forward primer for amplification was 5′-FAM-TCGCTCTTTCCGCTTCTTCG-3′, and the reverse primer for amplification was 5′-Biotin-TTCGCACACACGGACT-TACG-3′. Oligonucleotide sequences are listed in Table S2. Modifications to oligonucleotides included FITC (5′-FITC-sequence-3′), biotin (5′-biotin-iSp18 spacer-sequence-3′), and Cy5 (5′-Cy5-sequence-3′). All aptamer pools and aptamers were annealed before use by diluting to 1−10 $\mu$M in SELEX wash buffer (SELEX WB), heating at 95 °C for 5 min, and snap-cooling on ice for 5 min. Dimers (e.g. SCOReD) were annealed by combining T linker aptamer (e.g. SCORe.50-30T) and A linker aptamer (e.g. SCORe.50-30A) sequences at 25 $\mu$M in SELEX WB, heating at 95 °C for 5 min, and snap-cooling on ice for 5 min.

**Buffers.** SELEX wash buffer (SELEX WB) was prepared as previously described.[13] Binding buffer contained 0.1 mg/mL of yeast tRNA (Invitrogen) (tRNA), 0.1 mg/mL of salmon sperm DNA (Invitrogen) (SS DNA), and 2% of MACS BSA solution (Miltenyi Biotec).

**Recombinant Proteins.** BA.1 SARS-CoV-2 S protein S1 domain (ACROBiosystems S1N-C52Ha), BA.1 SARS-CoV-2 S protein trimer (ACROBiosystems SPN-C52Hz), BA.1 SARS-CoV-2 S protein NTD (ACROBiosystems SPD-C522df), BA.1 SARS-CoV-2 S protein RBD (ACROBiosystems SPD-C522e), BA.2 SARS-CoV-2 S protein RBD (ACROBiosystems SPD-C522g), SARS-CoV S1 protein (ACROBiosystems S1N−S52H5), human Axl (tyrosine-protein kinase receptor UFO) (ACROBiosystems AXL-H5226), and recombinant human CD8A protein (Sino Biological 10980-H08H) were purchased in a lyophilized form. All proteins contained His-tag. Omicron variant (BA.1) S1, S trimer, NTD, and RBD contained the following


https://doi.org/10.1021/acs.analchem.2c01993
Anal. Chem. XXXX, XXX, XXX−XXX

mutations: A67V, HV69-70del, T95I, G142D, VYY143-145del, N211del, L212I, ins214EPE, G339D, S371L, S373P, S375F, K417N, N440K, G446S, S477N, T478K, E484A, Q493R, G496S, Q498R, N501Y, Y505H, T547K, D614G, H655Y, N679K, P681H, N764K, D796Y, N856K, Q954H, N969K, and L981F. BA.2 RBD contained the following mutations: G339D, S371F, S373P, S375F, T376A, D405N, R408S, K417N, N440K, S477N, T478K, E484A, Q493R, Q498R, N501Y, and Y505H. Anti-SARS-CoV-2 spike RBD antibody, chimeric mAb, human IgG1 (ACROBiosystems S1N-M130), and anti-SARS-CoV-2 spike RBD broadly neutralizing antibody, human IgG1 (ACROBiosystems SPD-M265), were purchased in a lyophilized form. All proteins were reconstituted, aliquoted, and stored according to the manufacturer's recommendations. SARS-CoV-2 wild-type S protein trimer was kindly provided by the Institute of Protein Design (IPD) at the University of Washington.

**Viruses.** Inactivated (UV or heat-inactivated) SARS-CoV-2 (wild-type, Alpha, Beta, Delta, BA.1) and HCoV-OC43 virus samples at known concentrations were kindly provided by the NIH RADx-Radical Data Coordination Center (DCC) at the University of California San Diego and BEI Resources.

**Protein SELEX.** The protocol was based on the guidelines outlined by Wang et al.[22] and is outlined in Figure 1. Experimental conditions for seven rounds of SELEX are summarized in Table S1. Aptamers were partitioned by Dynabeads His-tag isolation and Pulldown (Novex by Life Technologies) on a rack magnet. Aptamers were amplified with Phusion high-fidelity DNA polymerase (NEB). Annealing, strand separation, and composition of buffers were described previously.[2]

**Next-Generation Sequencing (NGS) and Data Analysis.** The DNA pools from SELEX rounds were PCR-amplified with barcoded primers described in Table S3 using the MiSeq Reagent Kit v2 (300-cycles) (Illumina) and MiSeq System (Illumina) per the manufacturer's protocol. Sequence reads were analyzed as previously described.[13] NUPACK was used to predict the secondary structure of candidate aptamers.[23]

**Biolayer Interferometry (BLI).** Studies were performed with an Octet Red96 machine (Sartorius) at 25 °C and at 1000 rpm sample agitation. Presoaked Ni-NTA (NTA) sensors were rinsed in 1% BSA, 0.1 mg/mL tRNA, 0.1 mg/mL SS DNA, and 0.01% Tween-20 SELEX WB ("diluent") for 100 s. For experiments containing nasal swab in buffer, nasal swab samples were collected as previously described and spiked into diluent.[14] Next, tips were loaded with a 50 nM His-tagged protein until the signal reached a 3.5 nm signal threshold. Subsequently, tips were cross-linked in 0.1 M EDC 0.025 M NHS in $H_2O$ for 60 s, quenched in 1 M ethanolamine PBS (pH 8.5) for 60 s, and rinsed in diluent for 100 s. Then, biosensors were baselined in diluent for another 100 s. After association with the protein of interest diluted to the desired concentration, sensor tips were returned to the baseline diluent well for dissociation. Data were analyzed with Octet Data Analysis 9.0 (Sartorius). Kinetic values were determined from a global fit of several curves generated from serial dilutions of the protein with a 1:2 binding model (heterogeneous ligand). The $K_{D1}$ describes the rate of the initial binding, and the $K_{D2}$ describes the rate of a second binding event after the initial binding.

**Aptamer Round Pool Binding Assay.** The protocol was conducted using an ELISA-like plate binding assay, as previously described.[13] In brief, 96-well plates were coated overnight with the protein of interest. After washing and blocking wells with 5% BSA, 0.1 mg/mL tRNA, 0.1 mg/mL SS DNA, and 0.01% Tween-20 SELEX WB, fluorescein-labeled aptamer pools were incubated in the wells (30 min, RT) before staining with HRP antifluorescein antibody for detection with the TMB substrate. Aptamer binding was quantified by UV absorbance with measurements at 450 nm.

**Protein-Binding Plate Assay.** Nunc MaxiSorp flat-bottom 96-well plates (Thermo Fisher Scientific) were coated with 50 nM protein (except Omicron S trimer at 25 nM) at 4 °C overnight. Then, wells were washed four times with wash buffer (0.5% BSA, 0.01% Tween-20 SELEX WB). Next, wells were incubated with blocking buffer (5% BSA, 0.1 mg/mL tRNA, 0.1 mg/mL SS DNA, 0.01% Tween-20 SELEX WB) for 1.5 h at room temperature. After the blocking buffer removal via flick and tap, 100 nM biotin-labeled aptamer pools or control biotin-labeled aptamer in binding buffer was incubated for 30 min at room temperature. Then, the plate was washed four times with wash buffer and stained with Pierce high sensitivity streptavidin-HRP (1:16 000 1 mg/mL, Thermo Scientific 21130) for 1 h at room temperature. Lastly, the plate was washed four times with wash buffer. Pierce TMB substrate kit (Thermo Scientific 1854050) was mixed at 1:1 according to the manufacturer's protocol and then added to wells and incubated at room temperature until the desired blue color was developed (5−30 min). 2 M sulfuric acid was added to each well to terminate the HRP reaction. The absorbance of the solution (yellow) was measured using the Infinite 200 PRO plate reader (Tecan) at 450 nm with 550 nm as a reference. The absorbance values of the groups were deducted from wells without aptamer and plotted.

**Gold Nanoparticle Synthesis.** Gold nanoparticles were prepared by the citrate synthesis method that involves sodium citrate reduction of tetrachloroauric acid, as previously described.[14]

**Gold Nanoparticle and Antibody Conjugation.** Antibody-conjugate gold nanoparticles were prepared by adapting a protocol from Wang et al.[24] Anti-RBD chimeric mAb human IgG1 antibody (ACROBiosystems S1N-M130) was activated with 10-fold excess Traut's reagent in 2 mM EDTA PBS (pH 8.0) for 1 h and then desalted by Zeba Spin Desalting Columns, 7K MWCO (Thermo Scientific).[24] The activated antibody (10 $\mu$g/mL) was added to 1 mL of gold nanoparticles and incubated for 5 min before the addition of 150 $\mu$M of thiol-PEG12-acid (Broadpharm BP-21916). After 2 h incubation, 0.25% BSA was added to the solution and further incubated for 5 min before use.

**LFA Dipstick Manufacturing.** The protocol was conducted as previously described,[14] with adjustments to the striped test lines: test line 1: 2 mg/mL polystreptavidin R (pSA) (Eagle Biosciences, # 10 120 030) in DPBS. Test line 2: 0.5 mg/mL anti-FITC antibody (BioLegend, #408302). Control line: 0.5 mg/mL antihuman IgG antibody (BioLegend #410701).

**Multiplex LFA.** Binding buffer (1% BSA, 0.1 mg/mL tRNA, 0.1 mg/mL SS DNA, 0.01% Tween-20), 25 nM biotinylated aptamer, 25 nM FITC-labeled aptamer, and 50 $\mu$L antibody-functionalized gold nanoparticles were prepared, and then the analyte was added to a total volume of 100 $\mu$L. The solution was incubated at RT for 20 min with rocking. Then, a lateral flow device was dipped into the solution for 15−20 min (entire volume absorbed). Lastly, the lateral flow devices were


https://doi.org/10.1021/acs.analchem.2c01993
Anal. Chem. XXXX, XXX, XXX−XXX

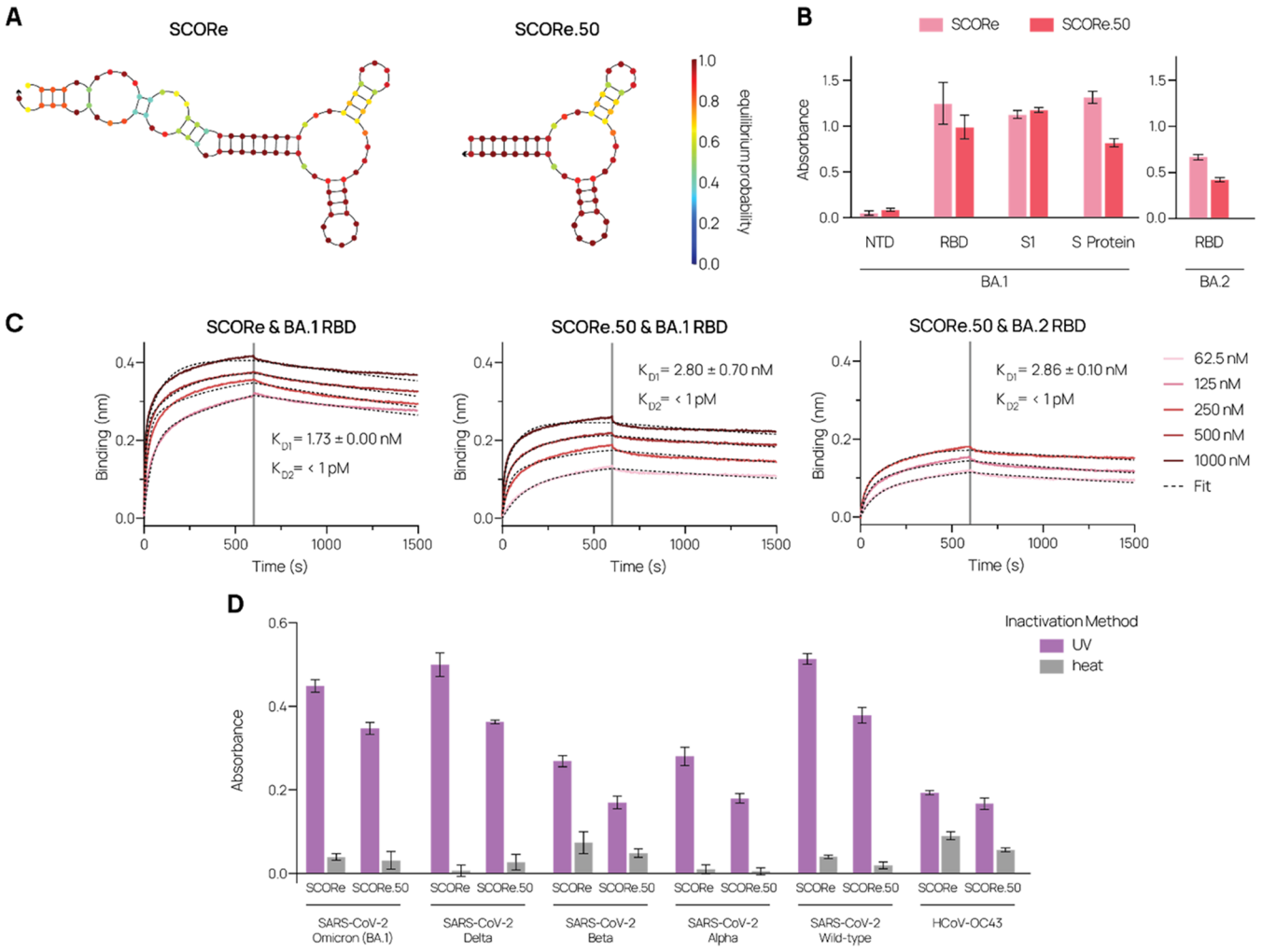


**Figure 2.** (A) Secondary structure prediction with the following conditions: 22 °C, 137 mM $Na^{+}$, 5.5 mM $Mg^{++}$. Arrows represent the 3′ end of the aptamer. (B, D) Proteins (B) or inactivated virus (D) adsorbed onto the surface are incubated with 100 nM biotinylated aptamer and stained with streptavidin-HRP with the detection of the HRP substrate TMB by UV absorbance. Bars indicate mean, and parentheses indicate S.D., $n = 3$. (C) Biolayer interferometry assessment of binding. His-tagged RBD was loaded on Ni-NTA biosensors and associated with SCORe-FITC or SCORe.50-biotin. The gray line indicates the switch from analyte association to dissociation after 600 s. $K_D$ values (mean ± S.D., $n = 3–4$) were determined from a global fit (dotted line) of the kinetic data at various concentrations of proteins for a 2:1 binding model.

dipped in 25 μL SELEX WB for 5 min (partial volume absorbed). For each strip, the average pixel values in the control band, test bands, and background (blank area between bands) were calculated. The band values were background-subtracted; then, the percent maximum signal across all strips for the same band was calculated. The LOD was determined from the lowest concentration of sample that was significantly higher than the negative control.

**Cell Culture.** The HEK293 ACE2 cell line stably expressing ACE2, generously provided by Dr. Jesse Bloom (Fred Hutchinson Cancer Research Center), was cultured in DMEM (Gibco) 10% FBS at 5% $CO_2$, 37 °C.[25]

**HEK293 ACE2 Competition.** His-tagged Omicron (BA.1) S trimer (25 nM) was incubated with 250 nM or 2.5 μM of SCOReD, 250 nM or 2.5 μM of SNAP1D, or 500 nM or 5 μM of SCORe.50 in binding buffer for 20 min at RT and then added to 200 000 HEK293T ACE2 cells for 20 min on ice. Cells were stained with anti-His-tag antibody-FITC (Invitrogen MA1-81891), and the fluorescence was read by a flow cytometer (Attune NxT, Invitrogen). The median mean fluorescence intensity (MFI) of experiment groups was background-subtracted from that of untreated cells. The percent inhibition was calculated by subtracting the experiment value from S-only average value and dividing it by the S-only average value.

**Virus Neutralization Studies.** HEK293 ACE2 cells (10 000) were plated in a 96-well plate and cultured to 75% confluence. Aptamers were annealed at 25 μM in DMEM 3 mM $MgCl_2$. Omicron variant (BA.1) SARS-CoV-2 S protein pseudotyped virus (12.5 μL (1:500 dilution in DMEM 3 mM $MgCl_2$ 2% FBS)) (ACROBiosystems PSSO-HLGB003) and indicated concentrations of aptamer or neutralizing antibody (ACROBiosystems SPD-M265) were incubated together in DMEM 3 mM $MgCl_2$ for 1 h at RT. Incubation media was removed, and virus was added for 2 h at 37 °C. Next, media was replaced with fresh complete media, and cells were incubated for 48 h. Cells were rinsed with 200 μL of 1× PBS, and then 40 μL of reporter lysis buffer (Promega) was added. The plate was frozen and then thawed before 20 μL of cell lysate was mixed with 100 μL of Luciferase assay reagent. Light was measured using the Infinite 200 PRO plate reader (Tecan) at a 1000 nm integration time. The relative light units (RLUs)


https://doi.org/10.1021/acs.analchem.2c01993
Anal. Chem. XXXX, XXX, XXX−XXX

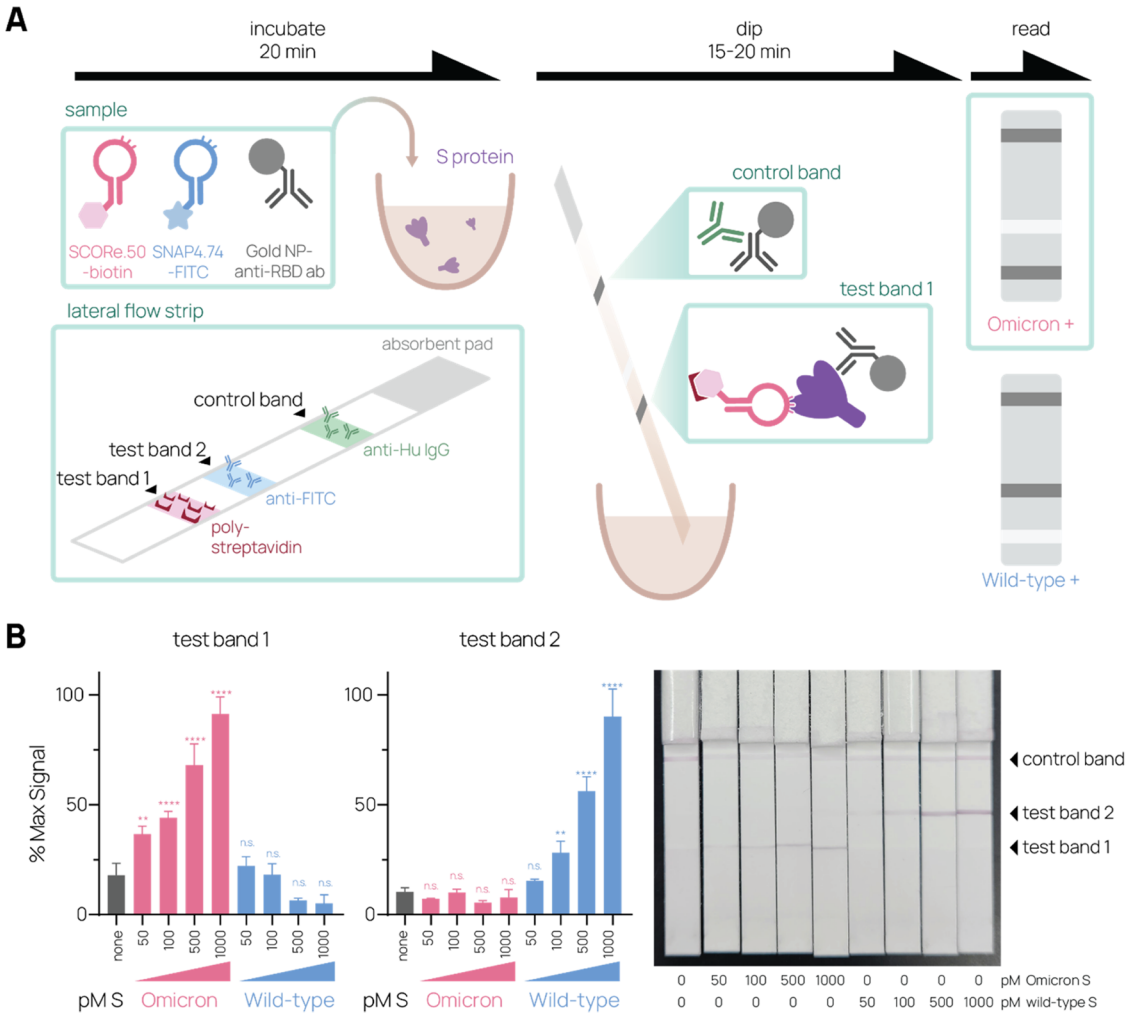


**Figure 3.** (A) LFA schematic. (B) Detection and differentiation between Omicron (BA.1) and wild-type SARS-CoV-2 S protein. "None" and "0 pM" indicate negative controls, which were treated identically as other samples except with no S protein added. Bars indicate mean. Parentheses indicate S.D. Statistical significance determined by one-way ANOVA with Dunnett correction; ** indicates $p < 0.01$, **** indicates $p < 0.0001$ when compared to no protein; $n = 3$ per experimental group. Representative images are shown.

of experiment groups were background-subtracted from that of untreated cells. The percent infectivity was calculated by normalizing to virus-only treatment group values.

## RESULTS AND DISCUSSION

**Aptamer Selection.** We designed a protein SELEX strategy to identify aptamers that bind to BA.1 S protein RBD. Our previous attempts using the RBD domain alone for SELEX were not successful, so we used SARS-CoV-2 BA.1 S1 protein for positive selection and SARS-CoV-2 BA.1 NTD for negative selection in later rounds. We conducted seven rounds of SELEX with increasing stringency, accomplished by increasing the amount of competitors (BSA, tRNA, SS DNA) and decreasing the amount concentration of aptamer pool and positive selection target Omicron (BA.1) S1 protein (Figure 1). For the last three rounds, we evaluated the binding of the fluorescein-labeled aptamer libraries from each selection round and observed binding to BA.1 S1 protein but not to NTD or Axl (tyrosine-protein kinase receptor UFO) (negative control protein), starting in round 5 (R5) and increasing significantly in round 7 (R7) (Figure S2). We analyzed libraries from rounds 3 through 7 by next-generation sequencing (NGS) and identified four aptamers of interest (named A1 to A4). A1 and A2 first appeared as early as round 3, while A3 appeared in round 4 and A4 in round 5. Between rounds 5 and 6, all motifs sharply increased in prevalence (Figure S3). We tested A1, A2, A3, and A4 and observed that A3 bound BA.1 S1 but not BA.1 NTD (Figure S1). Aptamers A1, A2, and A4 did not bind either S1 or NTD, and therefore were not further characterized.

**Characterization of SCORe (A3).** To determine the binding location of A3 on S1 protein, we evaluated A3 (Figure 2A) binding to Omicron S protein, S1, RBD, and NTD via an ELISA-like plate binding assay and found that A3 bound BA.1 RBD, BA.2 RBD, BA.1 S1, and BA.1 S protein (Figure 2B) but not BA.1 NTD. Given the binding location, we renamed A3 to **S**ARS-**C**oV-2 **O**micron **R**BD-binding Aptam**e**r (SCORe). The selection of an RBD-binding aptamer demonstrates that our SELEX strategy using negative selection against NTD was effective.

We compared the sequence of SCORe to other aptamers reported to bind the SARS-CoV-2 S protein at the RBD (CoV-2-RBD-1C, CoV-2-RBD-4C, CoV-2-6C3, nCoV-S1-Apt1, MSA5, and MSA52-T5)[17,19,20] and found no similarity between SCORe and the other sequences when compared with local alignment (Figure S4).[26]


https://doi.org/10.1021/acs.analchem.2c01993
Anal. Chem. XXXX, XXX, XXX−XXX

We next truncated the aptamer sequence to reduce the synthesis cost and potentially improve binding affinity.[9] The NUPACK secondary structure prediction of SCORe shows a stem formed by the constant sequences used for PCR amplification. We removed this stem in a 50-nt truncation called SCORe.50 (Figure 2A).

We used biolayer interferometry (BLI) to measure the binding affinity of SCORe and SCORe.50 for immobilized BA.1 RBD, revealing a $K_{D1}$ of 1.73 and 2.80 nM, respectively (Figure 2C). In addition, we show that SCORe.50 binds BA.2 RBD with a $K_{D1}$ of 2.86 nM. We did not observe the binding of RBD to biotinylated SCORe, SCORe.50, or SCORe.50-30T (SCORe.50 with a 5′ 30-nt thymidine linker) bound to streptavidin sensor surfaces. We hypothesize that the immobilization of the 5′ end of the aptamer may prevent conformational mobility required for binding. Lastly, we showed that SCORe and SCORe.50 bound to UV-inactivated BA.1 virus with 18.8-fold and 11.2-fold higher signals, respectively, than heat-inactivated BA.1 virus (Figure 2D).

We also evaluated aptamer binding to spike proteins of other variants of SARS-CoV-2 and other coronaviruses. We observed the binding of SCORe and SCORe.50 to wild-type RBD and wild-type S protein in plate binding assay (Figure S5A) but not by BLI (Figure S5B). We observed the binding of SCORe and SCORe.50 to Delta variant S1 protein, but not SARS-CoV S1 protein by plate binding assay (Figure S5C). We also observed the binding of both SCORe and SCORe.50 to UV-inactivated SARS-CoV-2 virus of different variants, including Omicron (BA.1), Delta, and wild-type (Figure 2D). SCORe and SCORe.50 did not bind as highly to heat-inactivated SARS-CoV-2 virus, presumably due to denaturation of S protein. Based on these results, we hypothesize that while SCORe can bind to RBD of several variants, such as wild-type and Delta variant, it binds with the highest affinity to Omicron variant RBD. Due to similarity in binding patterns and affinities on the same order of magnitude ($K_{D1}$ of 1.73 nM for SCORe and $K_{D1}$ of 2.80 nM for SCORe.50), we used SCORe.50 in subsequent studies.

**Multiplexed LFA with SCORe.50 and SNAP4.74.** We next applied SCORe.50 for multiplexed SARS-CoV-2 S protein detection in a lateral flow assay (LFA). Since SCORe.50 binds to Omicron S protein with higher affinity than wild-type S protein and our previously reported SNAP4.74 binds to wild-type S protein,[14] but not Omicron S protein, we hypothesized that we could use the two aptamers in a rapid detection format to differentiate between Omicron and wild-type S protein. We used SNAP4.74-fluorescein for wild-type S protein capture using anti-FITC antibody and SCORe.50-biotin for Omicron (BA.1) S protein capture using streptavidin (Figure 3A). To test our custom LFA, we incubated S protein with a solution containing biotinylated SCORe.50, FITC-labeled SNAP4.74, and anti-RBD IgG gold nanoparticles (Ab-AuNP). We then dipped into the solution a lateral flow strip with three immobilized bands: (1) polystreptavidin to capture SCORe.50-biotin, (2) anti-FITC antibody to capture SNAP4.74-FITC, and (3) anti-IgG antibody control to capture the remaining Ab-AuNPs. Ab-AuNPs bind to captured S proteins of either variant, allowing users to read results with the naked eye (Figure 3A). The lateral flow device differentiates between Omicron (BA.1) and wild-type S protein, with the detection limit as low as 50 pM of Omicron (BA.1) S protein and 100 pM of wild-type S protein (Figure 3B). Although SCORe.50 can bind wild-type S protein by plate binding studies, we did not observe the binding of SCORe.50-biotin with 1 nM wild-type S protein in lateral flow, even in the absence of SNAP4.74-FITC. We also show that SCORe.50-biotin can bind BA.1 RBD in a buffer-containing nasal swab by BLI, demonstrating the potential for patient nasal swab sample LFA (Figure S6). Our system is a proof-of-concept for a modular aptamer-based LFA system for differentiation between SARS-CoV-2 variants or diseases with similar symptoms, such as influenza. Because disease severity differs between variants,[27] an LFA system that can distinguish between SARS-CoV-2 variants may provide information useful for patient care and disease epidemiology.

**Pseudovirus Neutralization by SCORe.50 and SCOReD.** Multivalent aptamers have previously been shown to have a tighter affinity for their target protein.[10] A trimeric RNA aptamer was shown to neutralize wild-type SARS-CoV-2 entry to cells.[28] Therefore, designed SCORe.50 dimers that connect two SCORe.50 with a 12-, 20-, or 30-nt stretch of A−T complementary binding to augment binding affinity for Omicron RBD (Figure S7A). We first show costaining between fluorescently labeled SCORe.50 and BA.1 RBD binding to ACE2-overexpressing cells (Figure S7B). We observe no correlation with negative control aptamer (SNAP1.50), which binds wild-type NTD. Next, we screened the three dimer types by flow cytometry for competition with BA.1 S protein to ACE2-overexpressing HEK293 cells. We found that 20 A/T and 30 A/T linker length dimers were slightly more effective in reducing the binding of S protein than dimers with 12 A/T (Figure S7C). We also tested the binding of dimers to BA.1 RBD by BLI and observed similar binding patterns and affinities for each (Figure S7D). We selected the 30 A/T linker length SCORe.50 dimer (SCOReD) to focus on in the following experiments (Figure 4A).

We confirmed that SCOReD binds to BA.1 RBD with a $K_{D1}$ of 1.04 nM, similar to that of SCORe.50 (Figure 4B). SCOReD inhibited BA.1 S protein from binding to ACE2-overexpressing HEK293 cells, knocking down binding by 38.0% at a 10-fold molar excess of SCOReD to S and 69.0% at a 100-fold molar excess of SCOReD to S (Figure 4C). In comparison, monomeric SCORe.50 reduces binding by 38.5% at a 200-fold molar excess (equivalent to 100-fold molar excess of SCOReD). Analogous negative control dimer with wild-type-NTD-binding SNAP1.50 (SNAP1D) shows no inhibition. Lastly, we show that SCORe.50 and SCOReD can block Omicron (BA.1) S-pseudotyped virus entry (OPV) to ACE2-overexpressing HEK293 cells (Figure 4D). Cells were transduced with the OPV virus carrying the luciferase reporter gene in the presence of SNAP1D (control dimer), monomeric SCORe.50-30T, and SCOReD. Both SCORe.50-30T and SCOReD significantly reduced pseudovirus infection compared to control dimer. Both SCORe.50 and SCOReD significantly reduced infectivity in comparison to SNAP1D at 5 $\mu$M (Figure 4D) and 10 $\mu$M (Figure S8) of dimer or monomer molar equivalent. In particular, SCOReD reduced infection by 42.2 ± 4.4% at 5 $\mu$M (Figure 4D) and 71.1 ± 9.9% at 10 $\mu$M (Figure S8). To probe whether the SCOReD dimer provided an advantage over SCORe.50, we compared treatment with heterodimer composed of SCORe.50 and SNAP1.50 to treatment with SNAP1D and SCOReD. There was a significant difference between SNAP1D and SCOReD, but there was no significant difference between heterodimer and SNAP1D or heterodimer and SCOReD. This indicates that dimerization may not significantly augment the neutraliz-


https://doi.org/10.1021/acs.analchem.2c01993
Anal. Chem. XXXX, XXX, XXX−XXX

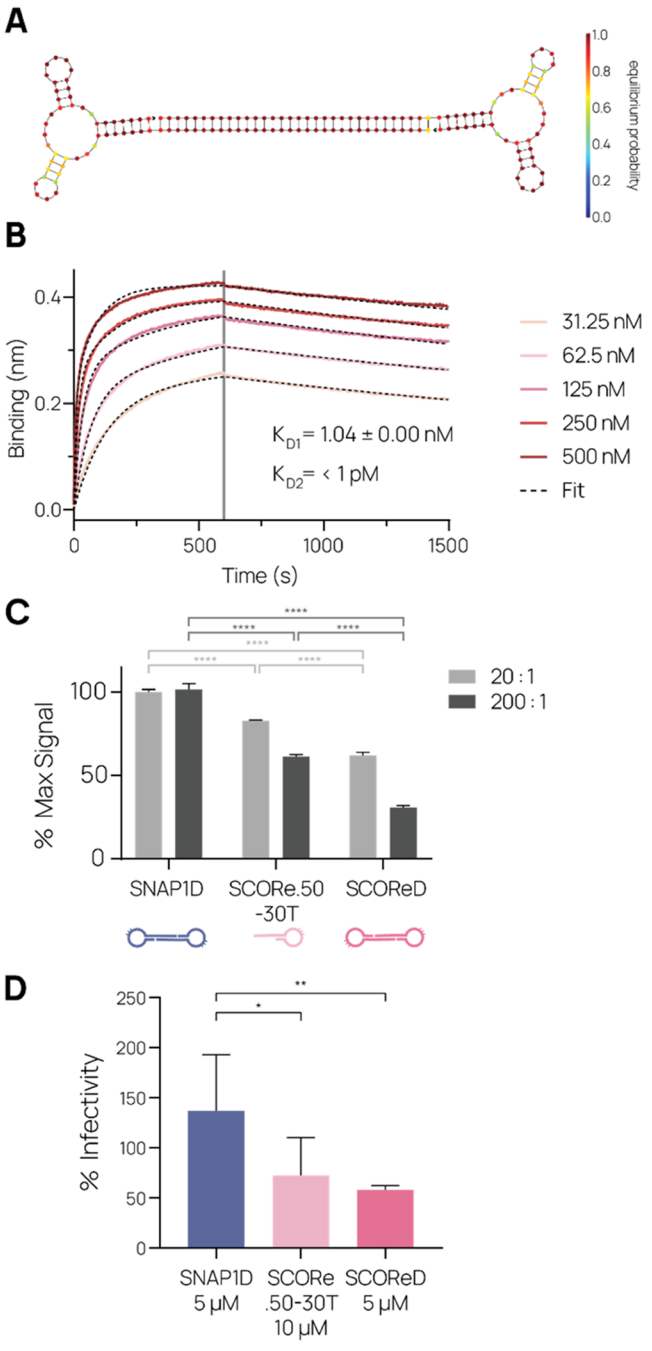


**Figure 4.** (A) Secondary structure prediction as described in Figure 2. (B) BLI characterization of SCOReD binding to immobilized RBD with experimental details and $K_D$ determination, as described in Figure 2. (C) ACE2-overexpressing HEK293 cells were incubated with 25 nM Omicron S protein and 250 nM or 2.5 $\mu$M of indicated dimer or 500 nM or 5 $\mu$M of monomeric SCORe.50-30T. S binding was measured by flow cytometry. Ratios (20:1, 200:1) indicate the molar ratio of monomeric aptamer units to S protein. Three technical replicates are shown. Bars represent mean, and parentheses represent S.D. **** denotes $p < 0.0001$ as determined by two-way ANOVA with Tukey's multiple comparison test. (D) Omicron S-pseudotyped virus infection of ACE2-overexpressing HEK293 cells in the presence of various aptamer constructs. Three biological replicates performed with four technical replicates each shown. Bars represent mean, and parentheses represent S.D. * denotes $p < 0.05$ and ** denotes $p < 0.01$ as determined by two-way ANOVA with Dunnett's multiple comparison test.

ing capabilities of SCORe.50 (Figure S9). Treatment with 10 $\mu$M SCOReD is less effective than with 10 or 100 nM of neutralizing antibody, which both achieved virtually complete neutralization (Figure S10).

## CONCLUSIONS

In this report, we discover and characterize SCORe, a high-affinity aptamer for the Omicron BA.1 and BA.2 S protein RBD domain. We apply a SCORe truncation, SCORe.50, together with our previously reported wild-type S protein-binding aptamer, SNAP4.74, in a multiplexed lateral flow assay and demonstrate the subnanomolar detection of and differentiation between Omicron (BA.1) and wild-type S. We demonstrated that SCORe.50 and its dimer SCOReD can compete with ACE2 for binding to Omicron (BA.1) S and inhibit pseudovirus infection. We use SCORe in rapid lateral flow assays and pseudovirus neutralization, demonstrating its versatile uses and potential for diagnostic and therapeutic applications.

## ASSOCIATED CONTENT

### Supporting Information

The Supporting Information is available free of charge at https://pubs.acs.org/doi/10.1021/acs.analchem.2c01993.

Selection conditions (Table S1), aptamer sequences (Table S2), supplemental binding experiments (Figures S1, S2, and S5−S7), NGS (Figure S3), local alignment (Figure S4), and supplemental pseudovirus inhibition studies (Figures S8−S10) (PDF)

## AUTHOR INFORMATION


### Corresponding Author

**Suzie H. Pun** − *Department of Bioengineering, University of Washington, Seattle, Washington 98195, United States;* orcid.org/0000-0003-1443-4996; Email: spun@uw.edu

### Authors

**Lucy F. Yang** − *Department of Bioengineering, University of Washington, Seattle, Washington 98195, United States*

**Nataly Kacherovsky** − *Department of Bioengineering, University of Washington, Seattle, Washington 98195, United States*

**Joey Liang** − *Department of Bioengineering, University of Washington, Seattle, Washington 98195, United States*

**Stephen J. Salipante** − *Department of Laboratory Medicine, University of Washington, Seattle, Washington 98195, United States*

Complete contact information is available at: https://pubs.acs.org/10.1021/acs.analchem.2c01993


### Author Contributions

The manuscript was written through contributions of all authors. All authors have given approval to the final version of the manuscript. L.F.Y., N.K., and S.H.P. designed the research; L.F.Y., N.K., and J.L. performed the research. L.F.Y. and J.L. conducted protein plate binding studies, SELEX, and round binding studies; L.F.Y. performed NGS; L.F.Y. and S.J.S. analyzed NGS data; L.F.Y. generated predicted secondary structures and performed BLI studies and LFA studies; L.F.Y. and N.K. designed aptamer modifications; N.K. performed flow cytometry studies; N.K. and L.F.Y. conducted pseudovirus neutralization studies; L.F.Y. designed the figures; and L.F.Y.,


https://doi.org/10.1021/acs.analchem.2c01993
Anal. Chem. XXXX, XXX, XXX−XXX

N.K., J.L., and S.H.P. wrote the paper with input from all authors.

### Funding

This work was supported by NIH 1U01AA029316.

### Notes

The authors declare no competing financial interest.

## ■ ACKNOWLEDGMENTS

The authors thank NIH RADx-Radical Data Coordination Center (DCC) at the University of California San Diego (funded under NIH grant # 1U24LM013755-01) for the inactivated SARS-CoV-2 samples deposited by the Centers for Disease Control and Prevention and obtained through BEI Resources, NIAID. The authors also thank Kelsi Penewit for NGS assistance, Ruixuan Wan for the gold nanoparticle synthesis assistance, Ian I. Cardle for helpful scientific discussions, Nuttada Panpradist for the lateral flow assay assistance, and Dr. Jesse Bloom for kindly providing HEK293 ACE2 cells.

## ■ ABBREVIATIONS

| | |
|---|---|
| SARS-CoV-2 | severe acute respiratory syndrome coronavirus 2 |
| S | spike protein |
| ACE2 | angiotensin-converting enzyme-2 |
| RBD | receptor-binding domain |
| NTD | N-terminal domain |
| LFA | lateral flow assay |
| SCORe | SARS-CoV-2 Omicron variant RBD-binding aptamer |

## ■ REFERENCES

(1) Singh, J.; Pandit, P.; McArthur, A. G.; Banerjee, A.; Mossman, K. *Virol. J.* **2021**, *18*, 166.

(2) Tao, K.; Tzou, P. L.; Nouhin, J.; Gupta, R. K.; de Oliveira, T.; Kosakovsky Pond, S. L.; Fera, D.; Shafer, R. W. *Nat. Rev. Genet.* **2021**, *22*, 757−773.

(3) Cameroni, E.; Bowen, J. E.; Rosen, L. E.; Saliba, C.; Zepeda, S. K.; Culap, K.; Pinto, D.; VanBlargan, L. A.; De Marco, A.; di Iulio, J.; et al. *Nature* **2022**, *602*, 664−670.

(4) Cele, S.; Jackson, L.; Khoury, D. S.; Khan, K.; Moyo-Gwete, T.; Tegally, H.; San, J. E.; Cromer, D.; Scheepers, C.; Amoako, D. G.; et al. *Nature* **2022**, *602*, 654−656.

(5) Walls, A. C.; Park, Y.-J.; Tortorici, M. A.; Wall, A.; McGuire, A. T.; Veesler, D. *Cell* **2020**, *181*, 281−292.

(6) (a) McCallum, M.; De Marco, A.; Lempp, F. A.; Tortorici, M. A.; Pinto, D.; Walls, A. C.; Beltramello, M.; Chen, A.; Liu, Z.; Zatta, F.; et al. *Cell* **2021**, *184*, 2332−2347. (b) Piccoli, L.; Park, Y.-J.; Tortorici, M. A.; Czudnochowski, N.; Walls, A. C.; Beltramello, M.; Silacci-Fregni, C.; Pinto, D.; Rosen, L. E.; Bowen, J. E.; et al. *Cell* **2020**, *183*, 1024−1042. (c) Harvey, W. T.; Carabelli, A. M.; Jackson, B.; Gupta, R. K.; Thomson, E. C.; Harrison, E. M.; Ludden, C.; Reeve, R.; Rambaut, A.; Peacock, S. J.; Robertson, D. L. *Nat. Rev. Microbiol.* **2021**, *19*, 409−424.

(7) Chen, A.; Yang, S. *Biosens. Bioelectron.* **2015**, *71*, 230−242.

(8) Baker, M. *Nature* **2015**, *521*, 274−276.

(9) (a) Abrego-Martinez, J. C.; Jafari, M.; Chergui, S.; Pavel, C.; Che, D.; Siaj, M. *Biosens. Bioelectron.* **2022**, *195*, No. 113595. (b) Idili, A.; Parolo, C.; Alvarez-Diduk, R.; Merkoçi, A. *ACS Sens.* **2021**, *6*, 3093−3101. (c) Lasserre, P.; Balansethupathy, B.; Vezza, V. J.; Butterworth, A.; Macdonald, A.; Blair, E. O.; McAteer, L.; Hannah, S.; Ward, A. C.; Hoskisson, P. A.; et al. *Anal. Chem.* **2022**, *94*, 2126−2133.

(10) Zhang, Z.; Pandey, R.; Li, J.; Gu, J.; White, D.; Stacey, H. D.; Ang, J. C.; Steinberg, C. J.; Capretta, A.; Filipe, C. D.; et al. *Angew. Chem., Int. Ed.* **2021**, *60*, 24266−24274.

(11) Peinetti, A. S.; Lake, R. J.; Cong, W.; Cooper, L.; Wu, Y.; Ma, Y.; Pawel, G. T.; Toimil-Molares, M. E.; Trautmann, C.; Rong, L.; et al. *Sci. Adv.* **2021**, *7*, No. eabh2848.

(12) (a) Aithal, S.; Mishriki, S.; Gupta, R.; Sahu, R. P.; Botos, G.; Tanvir, S.; Hanson, R. W.; Puri, I. K. *Talanta* **2022**, *236*, No. 122841. (b) Chen, H.; Park, S.-G.; Choi, N.; Kwon, H.-J.; Kang, T.; Lee, M.-K.; Choo, J. *ACS Sens.* **2021**, *6*, 2378−2385. (c) Zavyalova, E.; Ambartsumyan, O.; Zhdanov, G.; Gribanyov, D.; Gushchin, V.; Tkachuk, A.; Rudakova, E.; Nikiforova, M.; Kuznetsova, N.; Popova, L.; et al. *Nanomaterials* **2021**, *11*, 1394.

(13) Kacherovsky, N.; Yang, L. F.; Dang, H. V.; Cheng, E. L.; Cardle, I. I.; Walls, A. C.; McCallum, M.; Sellers, D. L.; DiMaio, F.; Salipante, S. J.; et al. *Angew. Chem.* **2021**, *133*, 21381−21385.

(14) Yang, L. F.; Kacherovsky, N.; Panpradist, N.; Wan, R.; Liang, J.; Zhang, B.; Salipante, S. J.; Lutz, B. R.; Pun, S. H. *Anal. Chem.* **2022**, *94*, 7278−7285.

(15) (a) Ellington, A. D.; Szostak, J. W. *Nature* **1990**, *346*, 818. (b) Robertson, D. L.; Joyce, G. F. *Nature* **1990**, *344*, 467−468. (c) Tuerk, C.; Gold, L. *Science* **1990**, *249*, 505−510.

(16) (a) Ferreira-Bravo, I. A.; DeStefano, J. J. *Viruses* **2021**, *13*, 1983. (b) Gupta, A.; Anand, A.; Jain, N.; Goswami, S.; Anantharaj, A.; Patil, S.; Singh, R.; Kumar, A.; Shrivastava, T.; Bhatnagar, S.; et al. *Mol. Ther. Nucleic Acids* **2021**, *26*, 321−332. (c) Liu, X.; Wang, Yl.; Wu, J.; Qi, J.; Zeng, Z.; Wan, Q.; Chen, Z.; Manandhar, P.; Cavener, V. S.; Boyle, N. R.; et al. *Angew. Chem., Int. Ed.* **2021**, *60*, 10273−10278. (d) Martínez-Roque, M. A.; Franco-Urquijo, P. A.; García-Velásquez, V. M.; Choukeife, M.; Mayer, G.; Molina-Ramírez, S. R.; Figueroa-Miranda, G.; Mayer, D.; Alvarez-Salas, L. M. *Anal. Biochem.* **2022**, *645*, No. 114633. (e) Shi, L.; Wang, L.; Ma, X.; Fang, X.; Xiang, L.; Yi, Y.; Li, J.; Luo, Z.; Li, G. *Anal. Chem.* **2021**, *93*, 16646−16654. (f) Sun, M.; Liu, S.; Wei, X.; Wan, S.; Huang, M.; Song, T.; Lu, Y.; Weng, X.; Lin, Z.; Chen, H.; et al. *Angew. Chem.* **2021**, *133*, 10354−10360.

(17) (a) Li, J.; Zhang, Z.; Gu, J.; Stacey, H. D.; Ang, J. C.; Capretta, A.; Filipe, C. D.; Mossman, K. L.; Balion, C.; Salena, B. J.; et al. *Nucleic Acids Res.* **2021**, *49*, 7267−7279. (b) Yang, G.; Li, Z.; Mohammed, I.; Zhao, L.; Wei, W.; Xiao, H.; Guo, W.; Zhao, Y.; Qu, F.; Huang, Y. *Signal Transduction Targeted Ther.* **2021**, *6*, 227.

(18) Schmitz, A.; Weber, A.; Bayin, M.; Breuers, S.; Fieberg, V.; Famulok, M.; Mayer, G. A. *Angew. Chem., Int. Ed.* **2021**, *60*, 10279−10285.

(19) Song, Y.; Song, J.; Wei, X.; Huang, M.; Sun, M.; Zhu, L.; Lin, B.; Shen, H.; Zhu, Z.; Yang, C. *Anal. Chem.* **2020**, *92*, 9895−9900.

(20) Zhang, Z.; Li, J.; Gu, J.; Amini, R.; Stacey, H.; Ang, J.; White, D.; Filipe, C.; Mossman, K.; Miller, M. *Chem. − Eur. J.* **2022**, *28*, No. e202200524.

(21) Sun, M.; Wu, Z.; Zhang, J.; Chen, M.; Lu, Y.; Yang, C.; Song, Y. *Nano Today* **2022**, *44*, No. 101499.

(22) Wang, T.; Yin, W.; AlShamaileh, H.; Zhang, Y.; Tran, P. H.-L.; Nguyen, T. N.-G.; Li, Y.; Chen, K.; Sun, M.; Hou, Y.; et al. *Hum. Gene Ther. Methods* **2019**, *30*, 1−16.

(23) Zadeh, J. N.; Steenberg, C. D.; Bois, J. S.; Wolfe, B. R.; Pierce, M. B.; Khan, A. R.; Dirks, R. M.; Pierce, N. A. *J. Comput. Chem.* **2011**, *32*, 170−173.

(24) Wang, X.; Mei, Z.; Wang, Y.; Tang, L. *Talanta* **2015**, *136*, 1−8.

(25) Crawford, K. H. D.; Eguia, R.; Dingens, A. S.; Loes, A. N.; Malone, K. D.; Wolf, C. R.; Chu, H. Y.; Tortorici, M. A.; Veesler, D.; Murphy, M.; et al. *Viruses* **2020**, *12*, 513.

(26) Madeira, F.; Pearce, M.; Tivey, A.; Basutkar, P.; Lee, J.; Edbali, O.; Madhusoodanan, N.; Kolesnikov, A.; Lopez, R. *Nucleic Acids Res.* **2022**, *50*, W276−W279.

(27) Lauring, A. S.; Tenforde, M. W.; Chappell, J. D.; Gaglani, M.; Ginde, A. A.; McNeal, T.; Ghamande, S.; Douin, D. J.; Talbot, H. K.; Casey, J. D.; et al. *BMJ* **2022**, *376*, No. e069761.

(28) Valero, J.; Civit, L.; Dupont, D. M.; Selnihhin, D.; Reinert, L. S.; Idorn, M.; Israels, B. A.; Bednarz, A. M.; Bus, C.; Asbach, B.; et al. *Proc. Natl. Acad. Sci. U.S.A.* **2021**, *118*, No. e2112942118.



https://doi.org/10.1021/acs.analchem.2c01993
*Anal. Chem.* XXXX, XXX, XXX−XXX